nature catalysis

SUPPLEMENTARY INFORMATION

https://doi.org/10.1038/s41929-018-0203-5

In the format provided by the authors and unedited.

# Identification of single-atom active sites in carbon-based cobalt catalysts during electrocatalytic hydrogen evolution

**Linlin Cao[1,4], Qiquan Luo[2,4], Wei Liu[1,4], Yue Lin[2], Xiaokang Liu[1], Yuanjie Cao[1], Wei Zhang[1], Yuen Wu[3], Jinlong Yang[2], Tao Yao[1*] and Shiqiang Wei[1*]**

[1]National Synchrotron Radiation Laboratory, University of Science and Technology of China, Hefei, China. [2]Hefei National Laboratory for Physical Sciences at the Microscale, University of Science and Technology of China, Hefei, China. [3]Department of Chemistry, Collaborative Innovation Center of Chemistry for Energy Materials, University of Science and Technology of China, Hefei, China. [4]These authors contributed equally: Linlin Cao, Qiquan Luo, Wei Liu
*e-mail: yaot@ustc.edu.cn; sqwei@ustc.edu.cn

Supplementary Information for

# Identification of single atomic active site in carbon-based cobalt catalysts during electrocatalytic hydrogen evolution

Linlin Cao[1†], Qiquan Luo[2†], Wei Liu[†1], Yue Lin[2], Xiaokang Liu[1], Yuanjie Cao[1], Wei Zhang[1], Yuen Wu[3], Jinlong Yang[2], Tao Yao[1]*, Shiqiang Wei[1]*

[1]National Synchrotron Radiation Laboratory, University of Science and Technology of China, Hefei 230029, P.R. China.

[2]Hefei National Laboratory for Physical Sciences at the Microscale, University of Science and Technology of China, Hefei 230026, P.R. China.

[3]Department of Chemistry, Collaborative Innovation Center of Chemistry for Energy Materials, University of Science and Technology of China, Hefei 230026, P.R. China.

†These authors contributed equally to this work

*e-mail: yaot@ustc.edu.cn; sqwei@ustc.edu.cn

**Contents:**

## Supplementary Figures

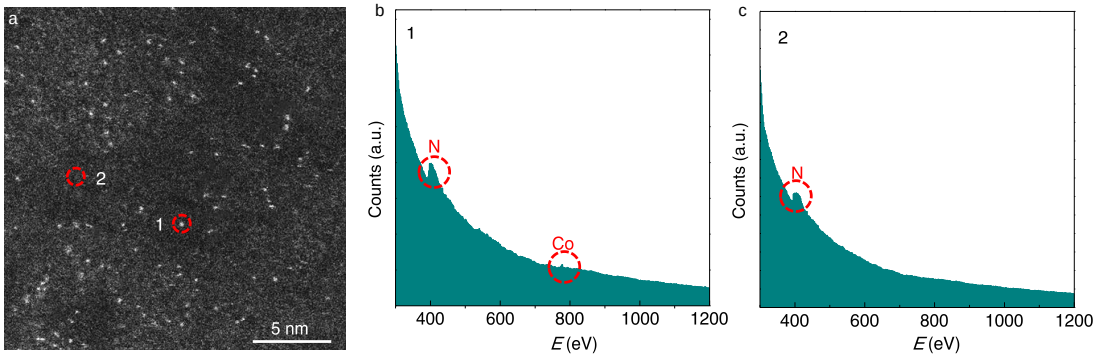


**Supplementary Figure 1.** (a) Atomic-resolution HAADF-STEM image of $Co_1$/PCN. (b) and (c) EELS spectra of N and Co elements from HAADF-STEM image in (a). When the electron beam was irradiated the bright dots (red circle), an obvious Co signal can be seen around 780 eV.

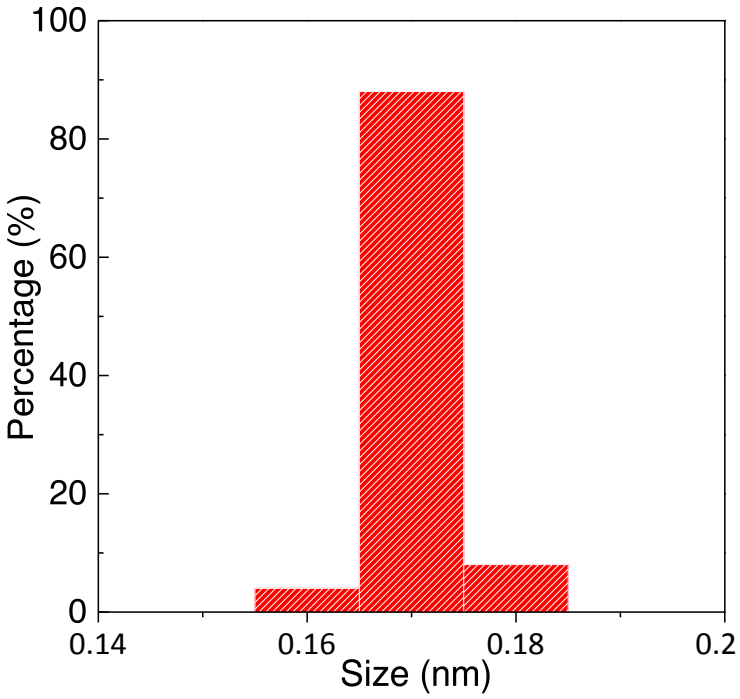


**Supplementary Figure 2.** The size distribution of single-atom Co. All of Co species on PCN is less than 0.2 nm, indicating that Co exists exclusively in atomic dispersion.

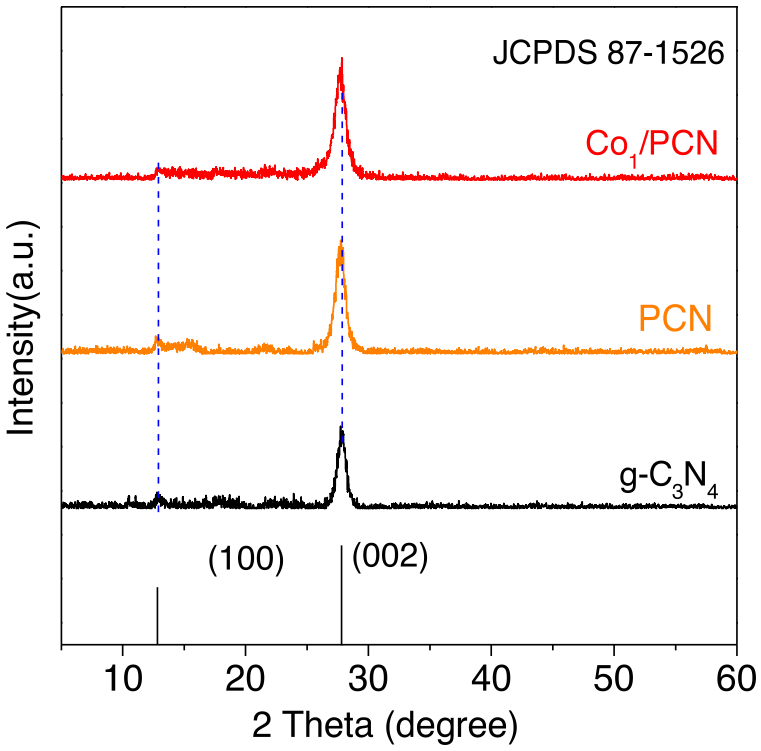


**Supplementary Figure 3.** XRD patterns of g-$C_3N_4$, PCN and $Co_1$/PCN. A diffraction peak at ca. 27 °corresponds to the (002) interplanar distance of 0.3 nm for the melon network. Another peak at 13.12 ° can be assigned to (100) in-planar ordering of tri-s-triazine.

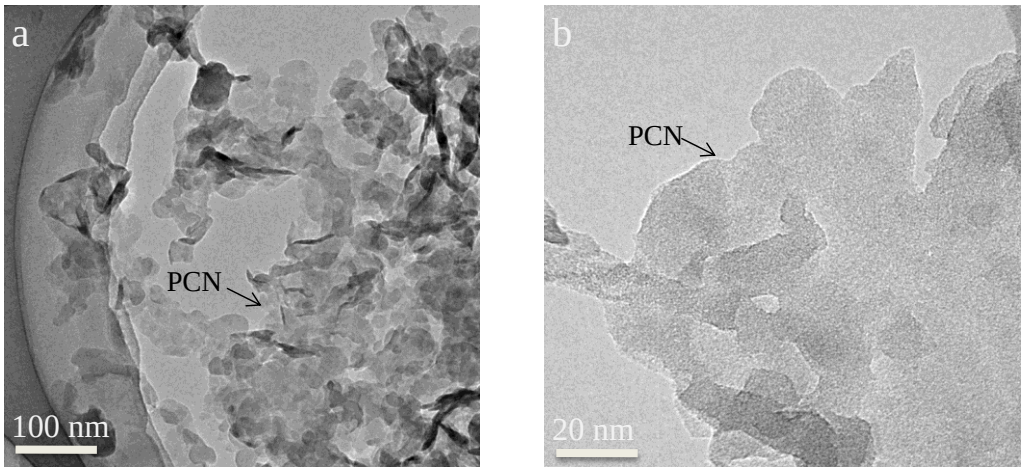


**Supplementary Figure 4.** (a) Low and (b) high magnification TEM images of $Co_1$/PCN electrocatalyst. The morphology of PCN nanosheet did not change after the introduction of Co species. No obvious Co-related nanoparticles were observed in the HRTEM image.

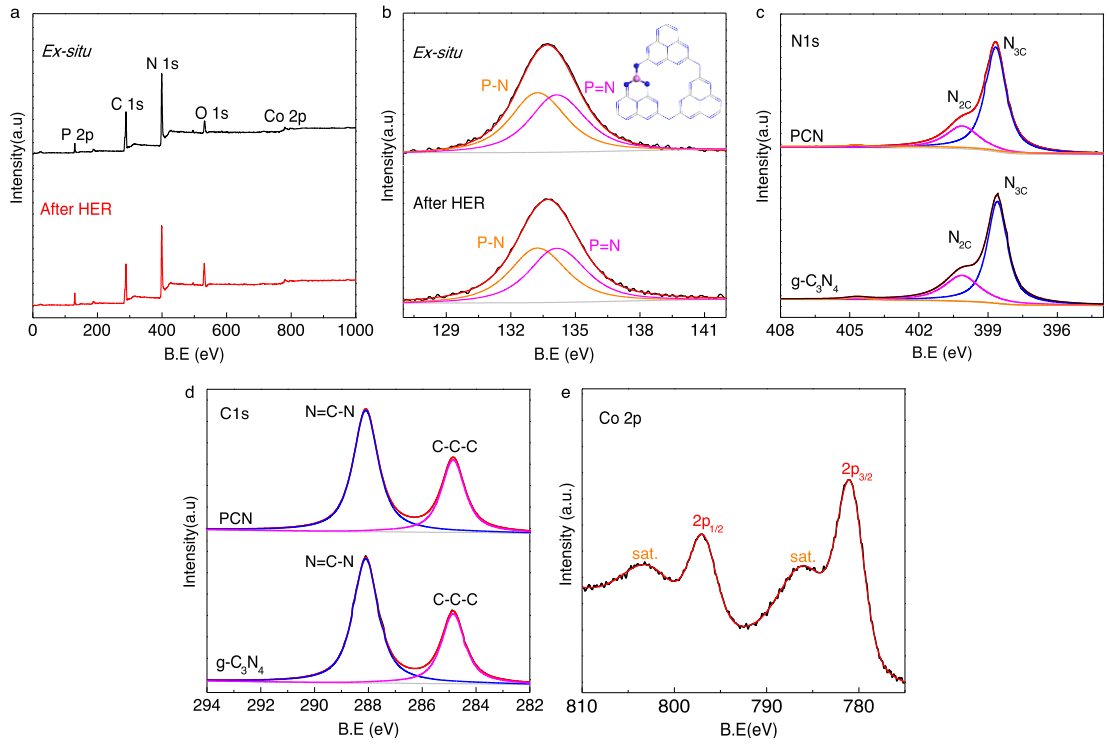


**Supplementary Figure 5.** (a) XPS survey spectra of the *ex-situ* catalyst and the catalyst has undergone HER test. (b) The high-resolution spectra of P 2p. Insert: the schematic model of P doping at C site. (c) The high-resolution N1s and (d) C1s XPS spectra. (e) Co 2p XPS spectra of the ex-situ catalyst. The XPS survey spectra, which indicate the existence of C, N, P, Co and O elements, in accordance with EDS-mapping results. The P 2p XPS spectra of the catalysts before and after HER display the same feature, possessing the peak at binding energy of 133.4 eV, corresponding to the coordination of P and N (P-O bonding would be ca. 1 eV higher while P-C bonding would be ca. 1-2 eV lower).[1] Furthermore, this XPS peak can be fitted with two contributions located at 133.0 eV and 133.9 eV, which are attributed to the P-N and P=N bond, respectively.[2,3] Thus, these results strongly suggest that P atoms most probably substitute C atoms in g-$C_3N_4$ to form P-N coordination.

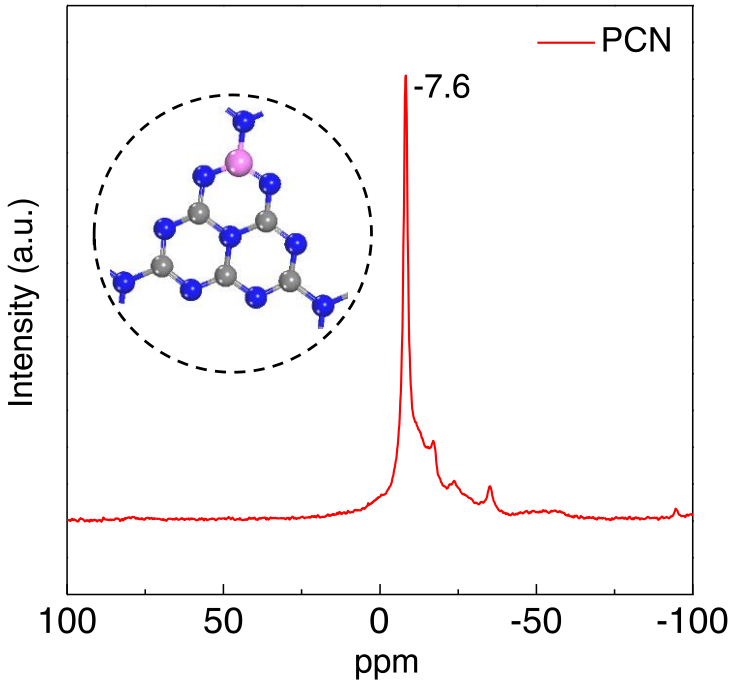


**Supplementary Figure 6.** $^{31}$P solid-state NMR spectra of PCN. The NMR spectrum possesses a major signal at -7.6 ppm, which clearly means that the P atoms have replaced C atoms in the g-$C_3N_4$ framework, forming P-N coordinations.[4,5]

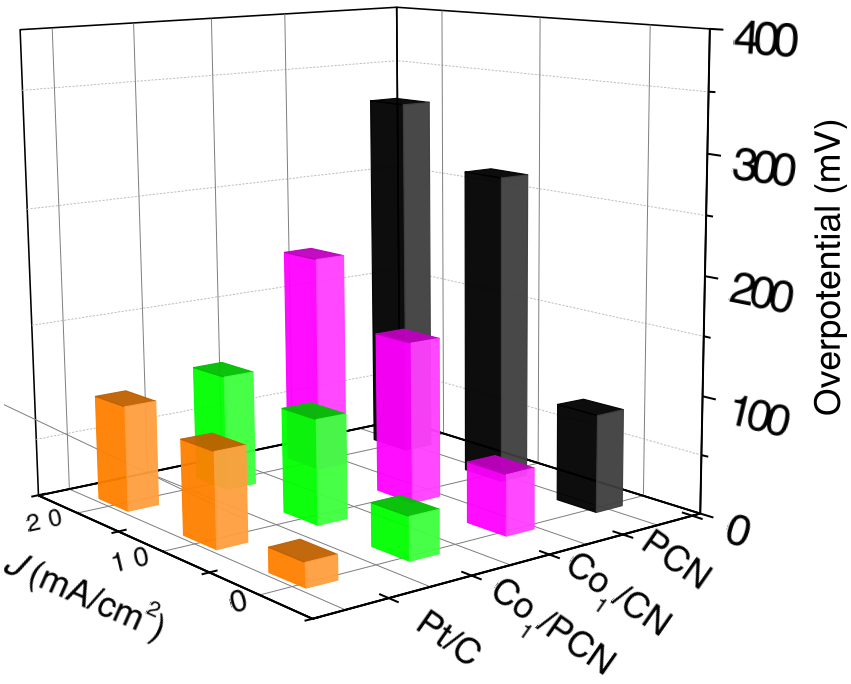


**Supplementary Figure 7.** The overpotentials obtained from HER polarization curves at the current densities of 0.5, 10, 20 mA $cm^{-2}$ for $Co_1$/PCN, $Co_1$/CN, Pt/C and PCN in $N_2$-saturated 1 M KOH electrolyte. As expected, the as-obtained $Co_1$/CN exhibited poor HER activity at 10 mA $cm^{-2}$ with a large overpotential of 138 mV, which is significantly inferior to that of the $Co_1$/PCN.

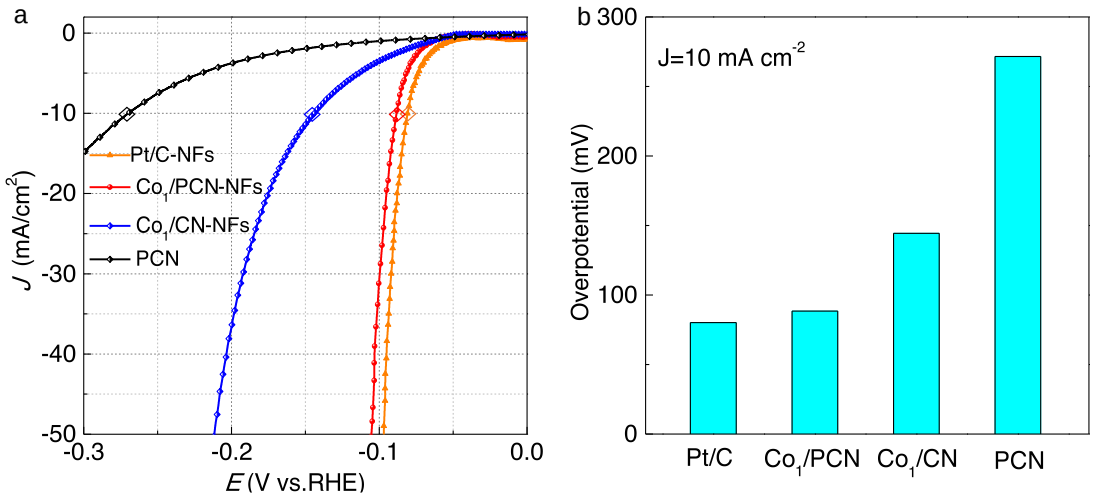


**Supplementary Figure 8.** (a) Electrocatalytic HER performance of the $Co_1$/PCN, $Co_1$/CN and Pt/C in $H_2$-saturated 1 M KOH electrolyte. (b) The corresponding overpotential at the current density of 10 mA $cm^{-2}$. The electrolyte solution was purged with $H_2$ for 30 min before each test. The electrochemical HER measurements in $N_2$ and $H_2$ saturated solutions are basically similar, indicating the reliability of experiments.

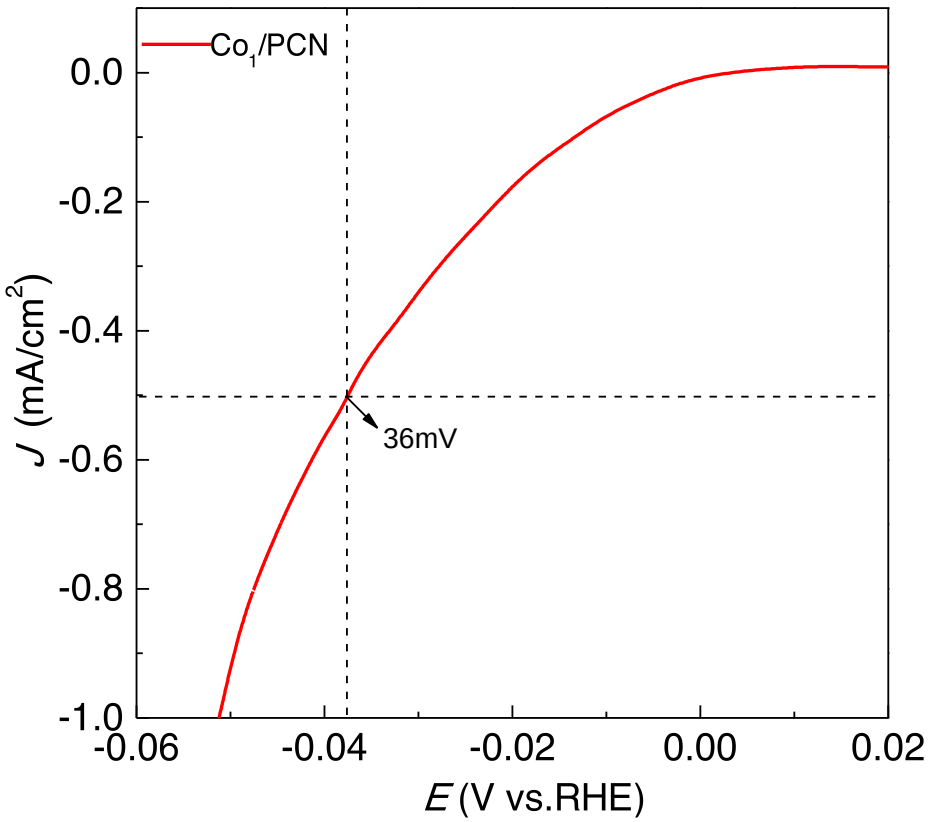


**Supplementary Figure 9.** The enlarged view of the LSV near the onset potential region, from Fig. 1e.

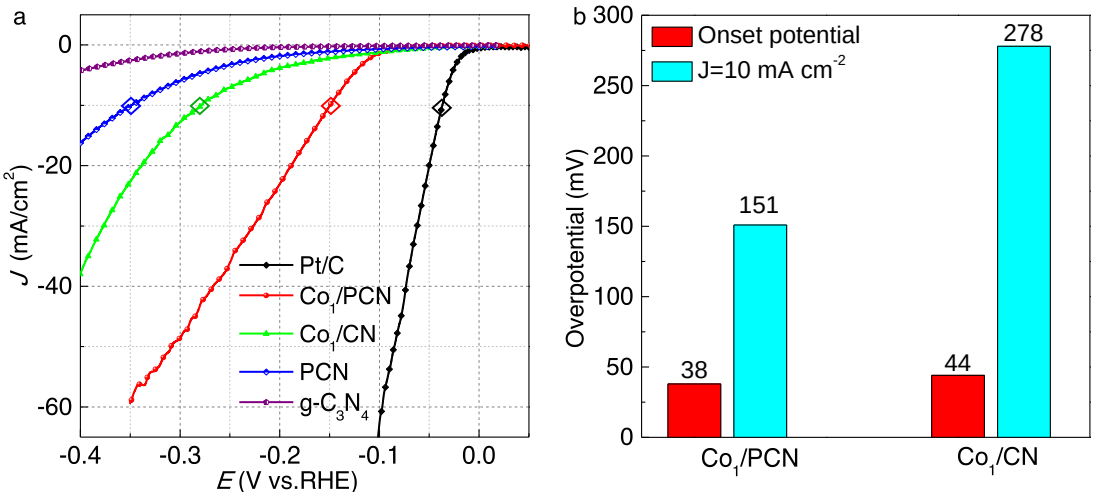


**Supplementary Figure 10.** (a) Electrocatalytic HER performance of $Co_1$/PCN and the controlled commercial Pt/C, $Co_1$/CN, PCN and pristine g-$C_3N_4$ in 0.5 M $H_2SO_4$ solution. (b) Corresponding overpotential for onset potential and the current density of 10 mA $cm^{-2}$ for $Co_1$/PCN and $Co_1$/CN.

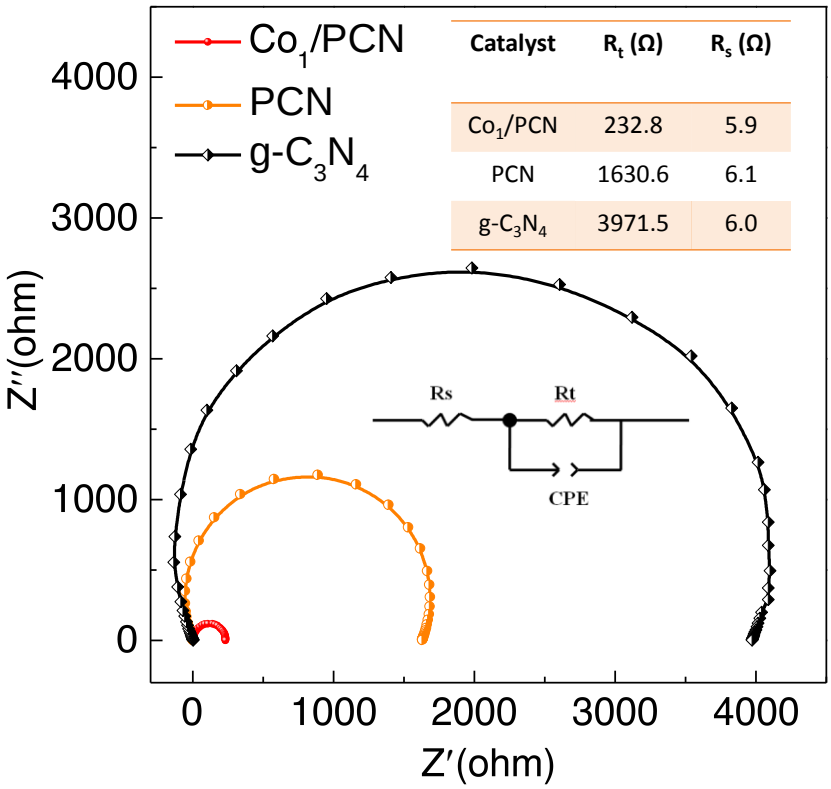


**Supplementary Figure 11.** EIS of the $Co_1$/PCN, $Co_1$/CN and PCN. Insert: the equivalent circuit diagram. It can be found that PCN shows the smaller diameter and the $R_t$ value in relation to g-$C_3N_4$. This suggests that the P doping can improve the interfacial charge transfer from electrode to electrolyte, which is critical for electrocatalytic HER.

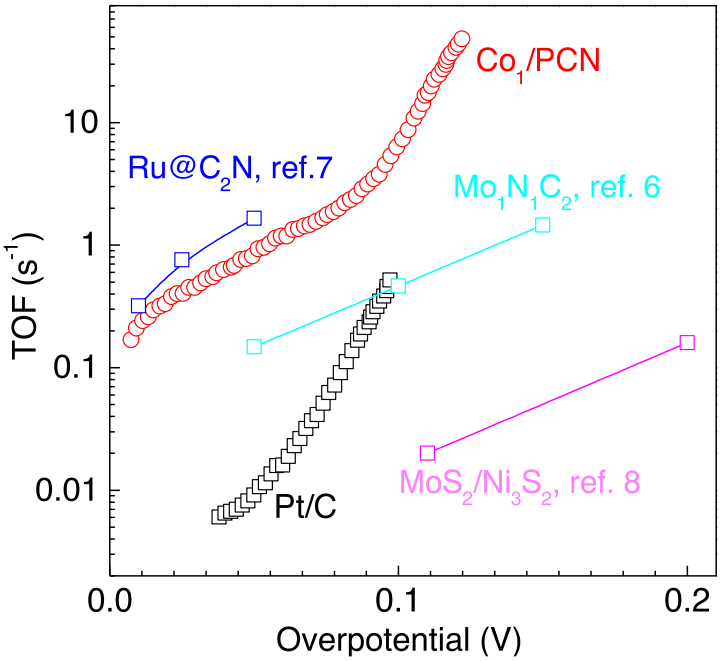


**Supplementary Figure 12.** TOF plots of the $Co_1$/PCN catalyst together with other recently reported catalysts. ($Mo_1N_1C_2$[6], $Ru@C_2N$[7], $MoS_2/Ni_3S_2$[8]). Data for $Co_1$/PCN, and Pt/C are from the present study.

The TOF of HER per Co site of the $Co_1$/PCN electrocatalyst was calculated according to the Equation S1. Assuming each cobalt atoms in the catalyst formed one active center. The numbers of Co atoms number in $Co_1$/PCN catalyst were calculated from the Co molar mass and the mass loading ($m_{Loading}$) on the NFs, which derived from the ICP. The Co content of catalyst revealed by ICP-AES measurement was ca. 0.3 wt%, thus, the mass loading is about 0.5 mg/cm$^2$.

$$\mathrm{TOF}(H_2/s) = \frac{\#\ \text{total hydrogen turnovers per geometric area}}{\#\ \text{active sites per geometric area}} \qquad (1)$$

The number of total hydrogen turnovers per geometric area was calculated from the current density for the HER-LSV polarization:

$$(|J|\frac{mA}{cm^2})(\frac{1C/s}{1000mA})(\frac{1\ mol\ e^-}{96453.8C})(\frac{1\ mol}{2e^-})(\frac{6.023\times10^{23}}{1\ mol\ H_2}) = 3.12\times10^{15}\frac{H_2/s}{cm^2}\ per\ \frac{mA}{cm^2} \qquad (2)$$

The upper limit of active site density is $1.38\times10^{16}$ Co site per cm$^2$

Finally, the current density from the HER-LSV polarization curve can be converted into values: $TOF=(3.12\times10^{15}/1.38\times10^{16})\times|J|=0.23|J|$

Particularly, at the overpotentials of 50 and 100 mV, the current density of HER are -0.94 and -26 mA cm$^{-2}$, respectively. Therefore, the TOF values of $Co_1$/PCN electrocatalyst were calculated to be:

$$TOF_{(50mV)} = 0.22\ H_2\ s^{-1}$$

$$TOF_{(100mV)} = 5.98\ H_2\ s^{-1}$$

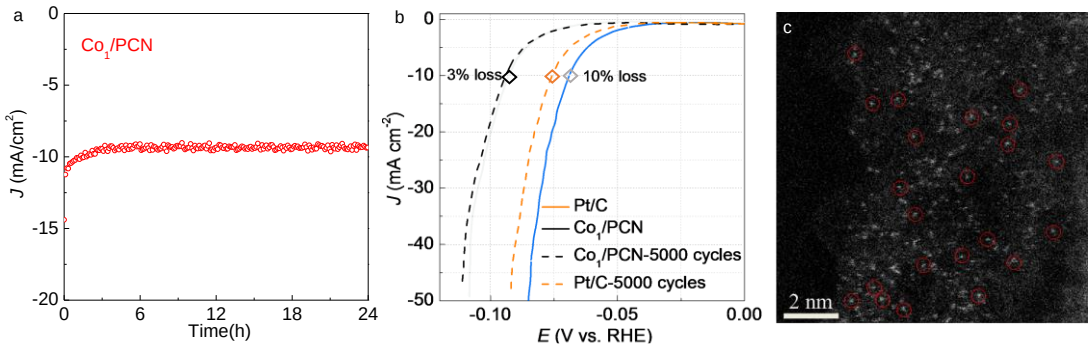


**Supplementary Figure 13.** (a) Long-time durability test in 1.0 M KOH solution at a stationary current density of 10 mA $cm^{-2}$ for 24 h. (b) Durability test of $Co_1$/PCN and Pt/C. The polarization curves were recorded before and after 5000 potential cycles in 1 M KOH electrolyte. (c) The atomic-resolution HAADF-STEM image of $Co_1$/PCN after HER test.

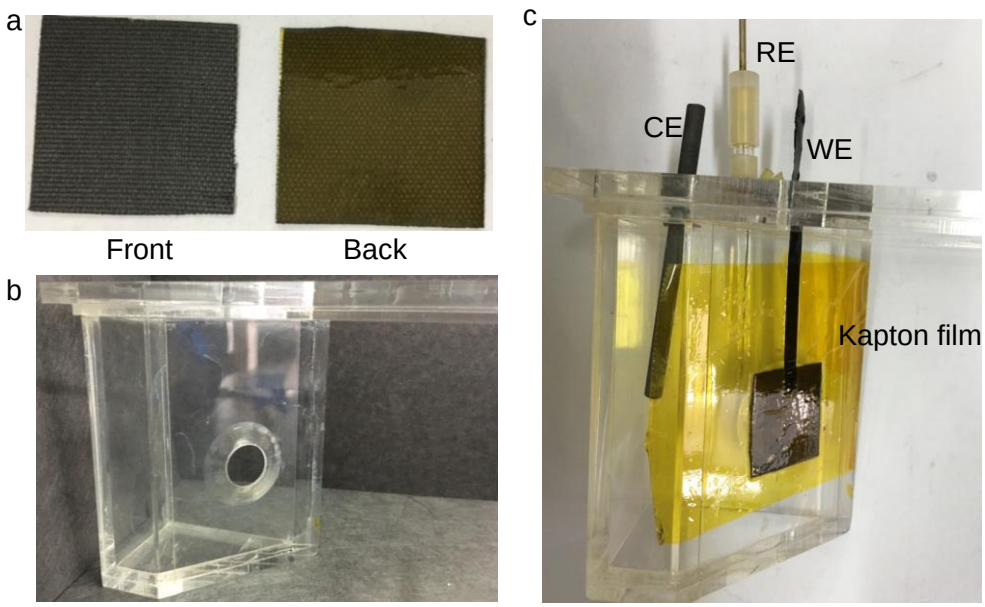


**Supplementary Figure 14.** The home-built electrochemical cell assembly parts. The back side of carbon cloth was pasted by Kapton film to avoid the leakage of electrolyte. The working electrode was fixed by Kapton film and connected with conductive carbon tape.

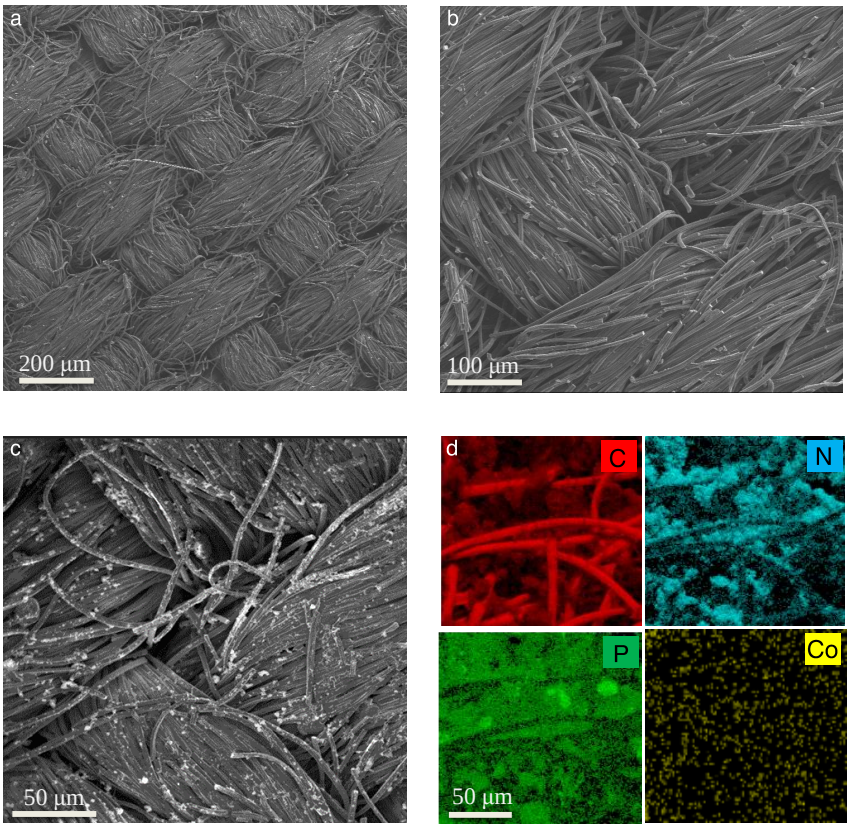


**Supplementary Figure 15.** SEM images for pure carbon paper (a), (b) and (c) working electrode. (d). Energy dispersive spectrometry (EDS) elemental mapping of $Co_1$/PCN deposited on carbon cloth.

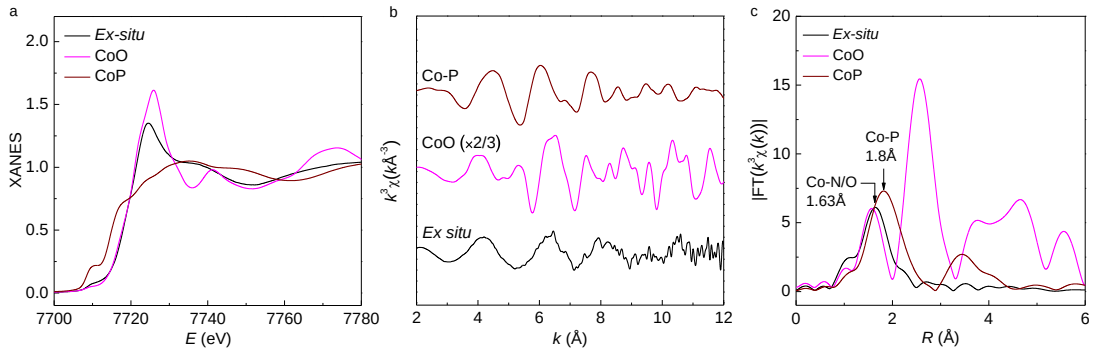


**Supplementary Figure 16.** This result can basically exclude the formation of Co-P coordination. (a) Co K-edge XANES spectra for ex-situ, CoO and CoP. (b) $k^3\chi(k)$ oscillations of Co K-edge EXAFS oscillation functions and (c) the corresponding FT curves. The XANES spectrum and EXAFS $k^3\chi$(k) function of the CoP reference are quite different from those of $Co_1$/PCN sample. Moreover, the FT curves of CoP reference is characterized by two main peaks at 1.8 Å and 2.6 Å, corresponding to the nearest Co-P and next Co-Co coordination, respectively, which are strikingly different from those of the $Co_1$/PCN sample. This result can basically exclude the formation of Co-P coordination.

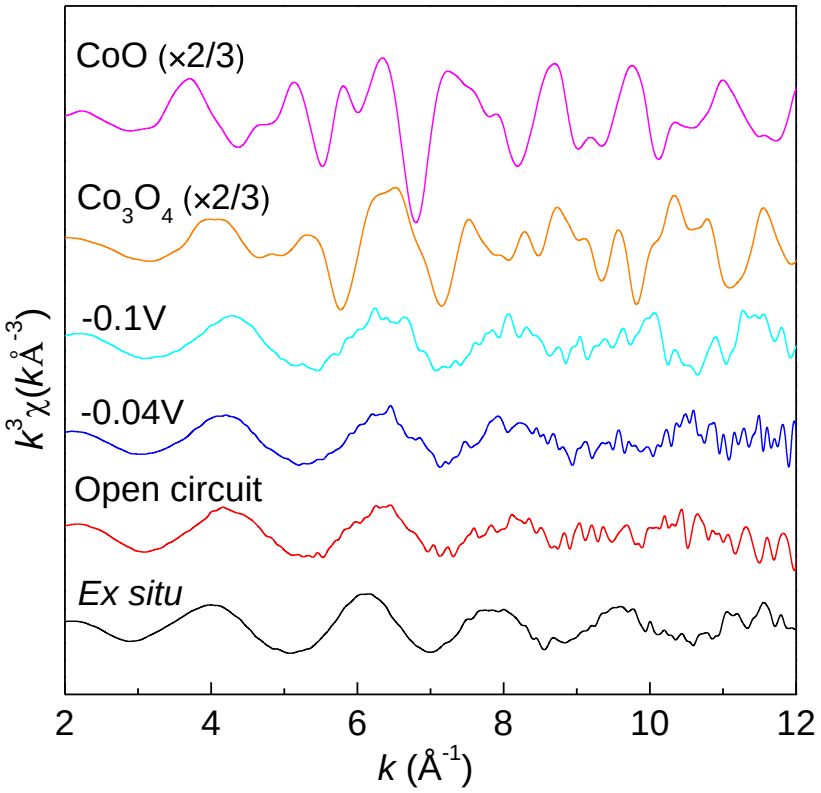


**Supplementary Figure 17.** $k^3\chi(k)$ oscillations of Co K-edge *operando* EXAFS analysis for the sample and references.

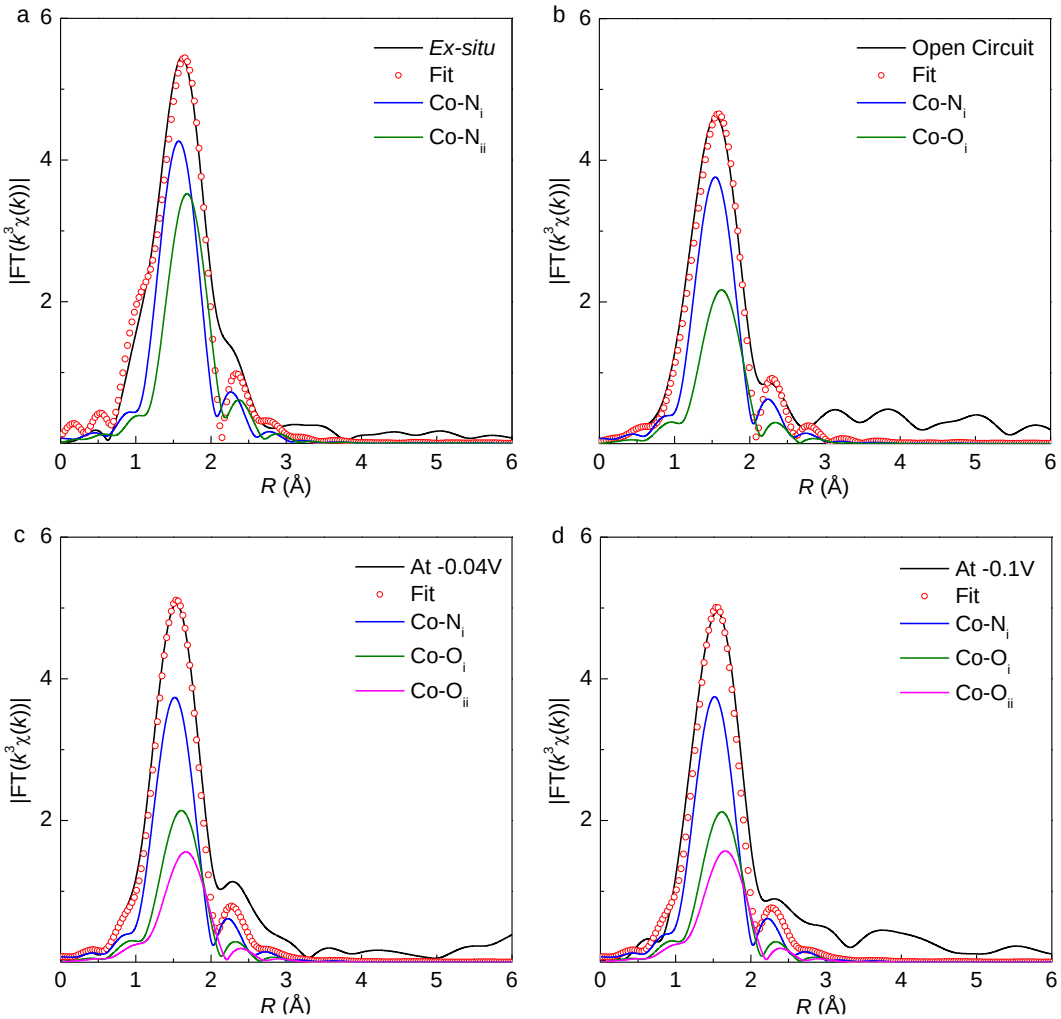


**Supplementary Figure 18.** The fitting curves of $k^3$-weighted EXAFS spectra for *ex situ* sample, at open circuit condition and at different overpotential of -0.04 V and -0.1 V versus RHE.

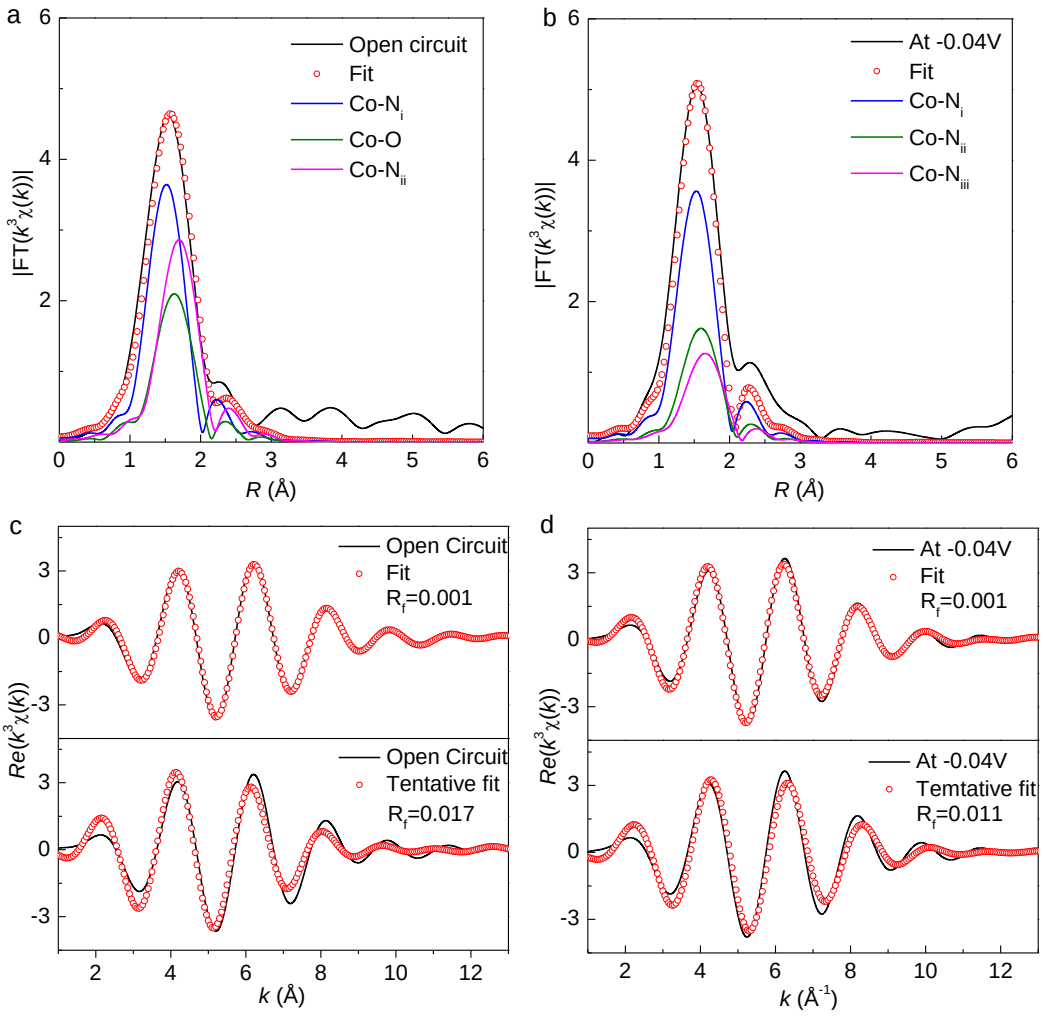


**Supplementary Figure 19.** The tentative fit for (a) the catalyst under open circuit and (b) at -0.4 V vs. RHE. (c) The $Re(k^3\chi(k))$ oscillation curves for open circuit and the tentative fit curves. (d) The $Re(k^3\chi(k))$ oscillation curves for at -0.04 V and the tentative fit curves. For the catalyst under open circuit condition, the FT-IR and XPS results have verified the OH adsorption on the Co site. Hence, we have added the Co-O scattering path in EXAFS fitting. We found that if the previous long Co-N bonds are considered, the fit became worse, as reflected by the large R-factor of 0.017. The additional EXAFS fitting with four Co-N paths for the sample under -0.04 V also conducted. Obviously, the quality of EXAFS fitting with four Co-N paths is worse, yielding *R*-factors of 0.011, larger than that 0.001 in the previous fitting with both Co-N and Co-O paths.

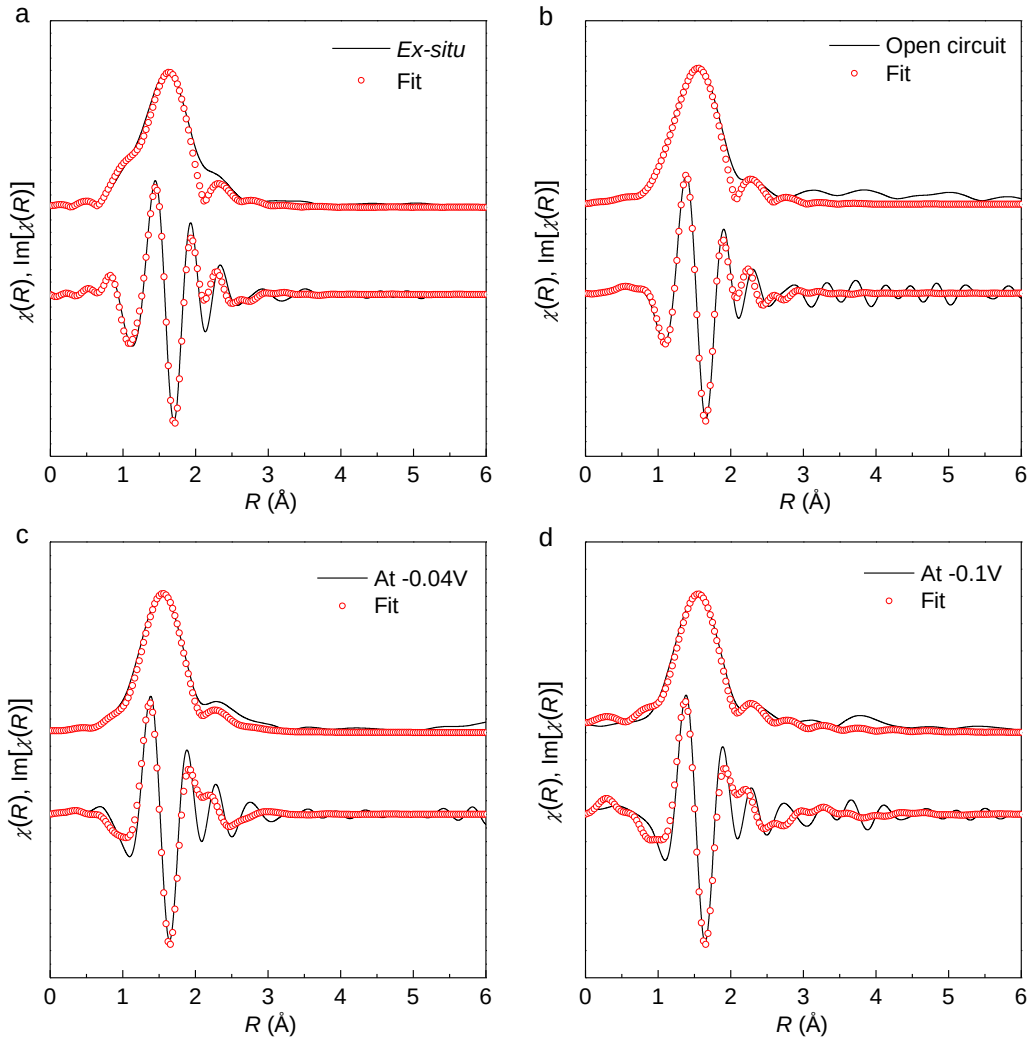


**Supplementary Figure 20.** The R-space curve-fitting of $Co_1$/PCN sample under different conditions (a) ex-situ sample, (b) at open circuit, (c) at -0.04 V and (d) at -0.1 V versus RHE.

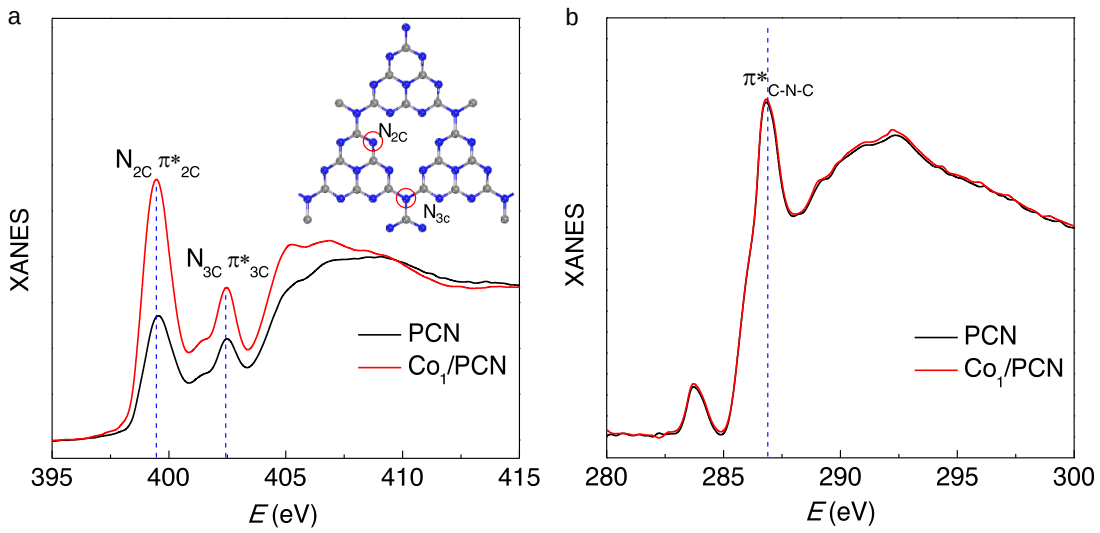


**Supplementary Figure 21.** N K-edge (b) C K-edge XANES spectra of $Co_1$/PCN and PCN. Significant variations in the peaks' intensity and position of π* regions can be observed in the N K-edge XANES spectra, while no obvious change can be found in C K-edge XANES spectra, indicating the strong interaction between N and Co atoms through orbital hybridization.[9,10]

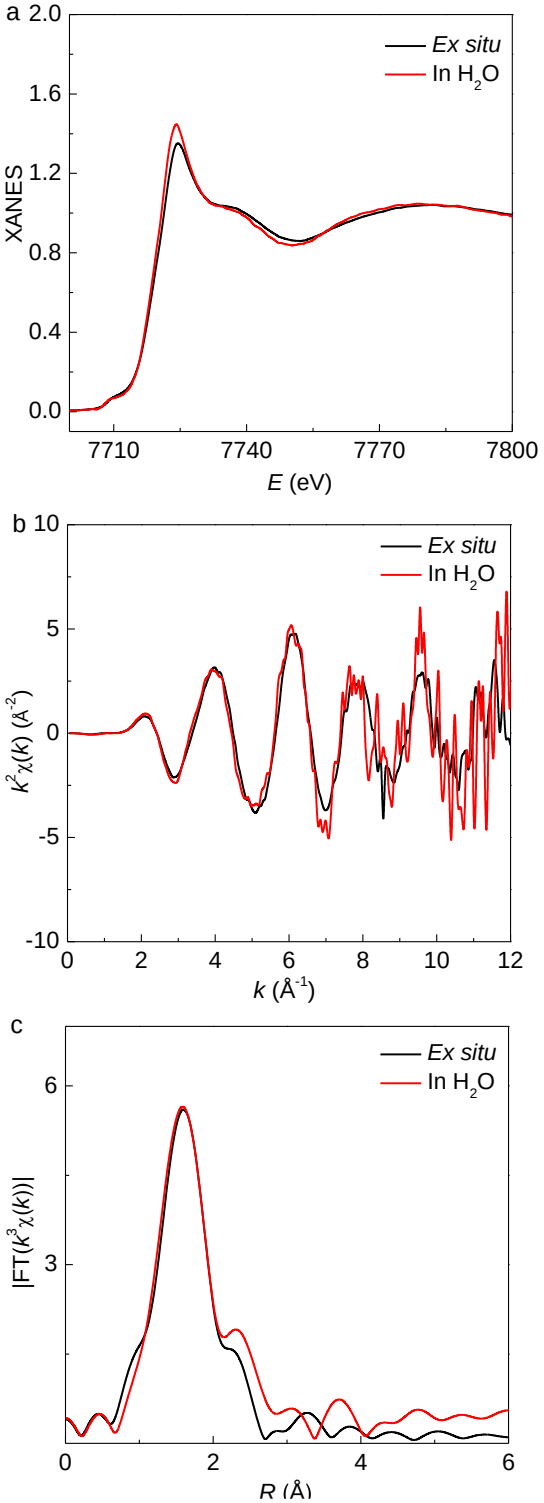


**Supplementary Figure 22.** (a) The Co K-edge XANES spectra. (b) $k^3\chi(k)$ oscillations of Co K-edge EXAFS analysis and (c) The corresponding $k^3$-weighted Fourier transforms (FT) spectra for *ex situ* catalyst and *operando* catalyst in neutral aqueous solution. It can be found that the XANES spectrum for the catalyst in aqueous solution is unchanged in relation to the *ex-situ* XANES data, precluding the adsorption of $H_2O$ molecule.

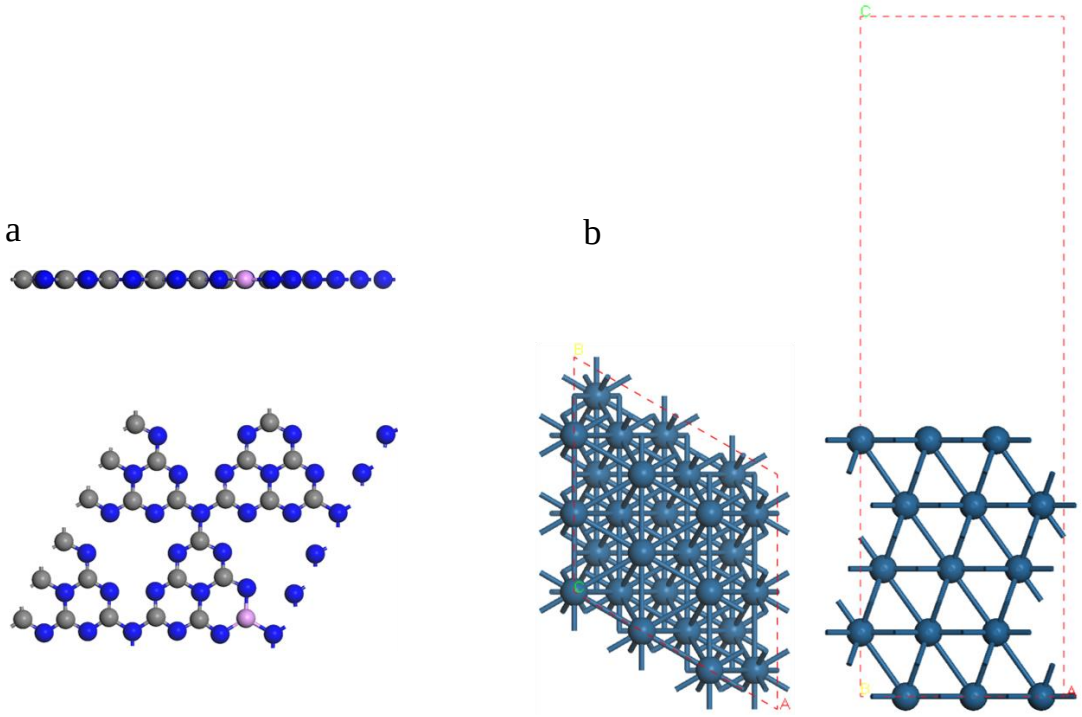


**Supplementary Figure 23.** Top and side views of (a) PCN and (b) the Pt (111) surface, C atoms in grey, N atoms in blue, P atom in pink and Pt atoms in dark blue, respectively.

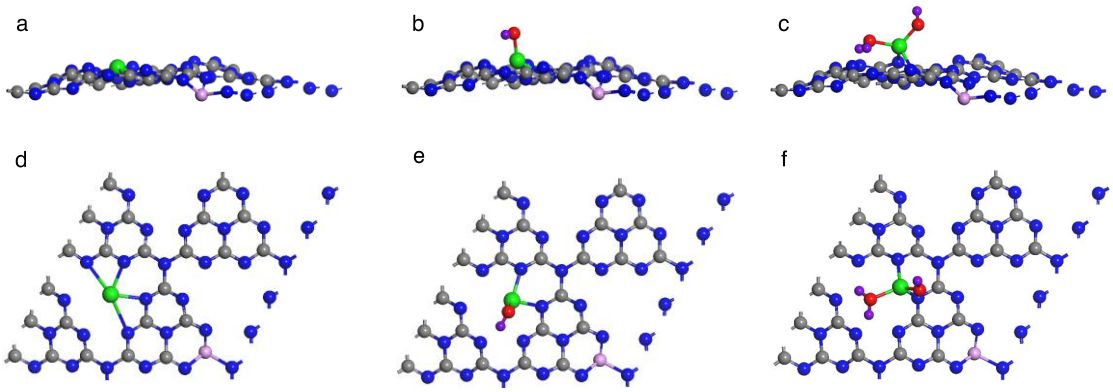


**Supplementary Figure 24.** Top and side views of atomic configuration for (a), (d) for *ex-situ* sample. (b), (e) Open circuit condition, and (c), (f) $H_2O$-Co-OH (Green, pink, grey, blue, Red and violet represent Co, P, C, N, O and H atoms), respectively.

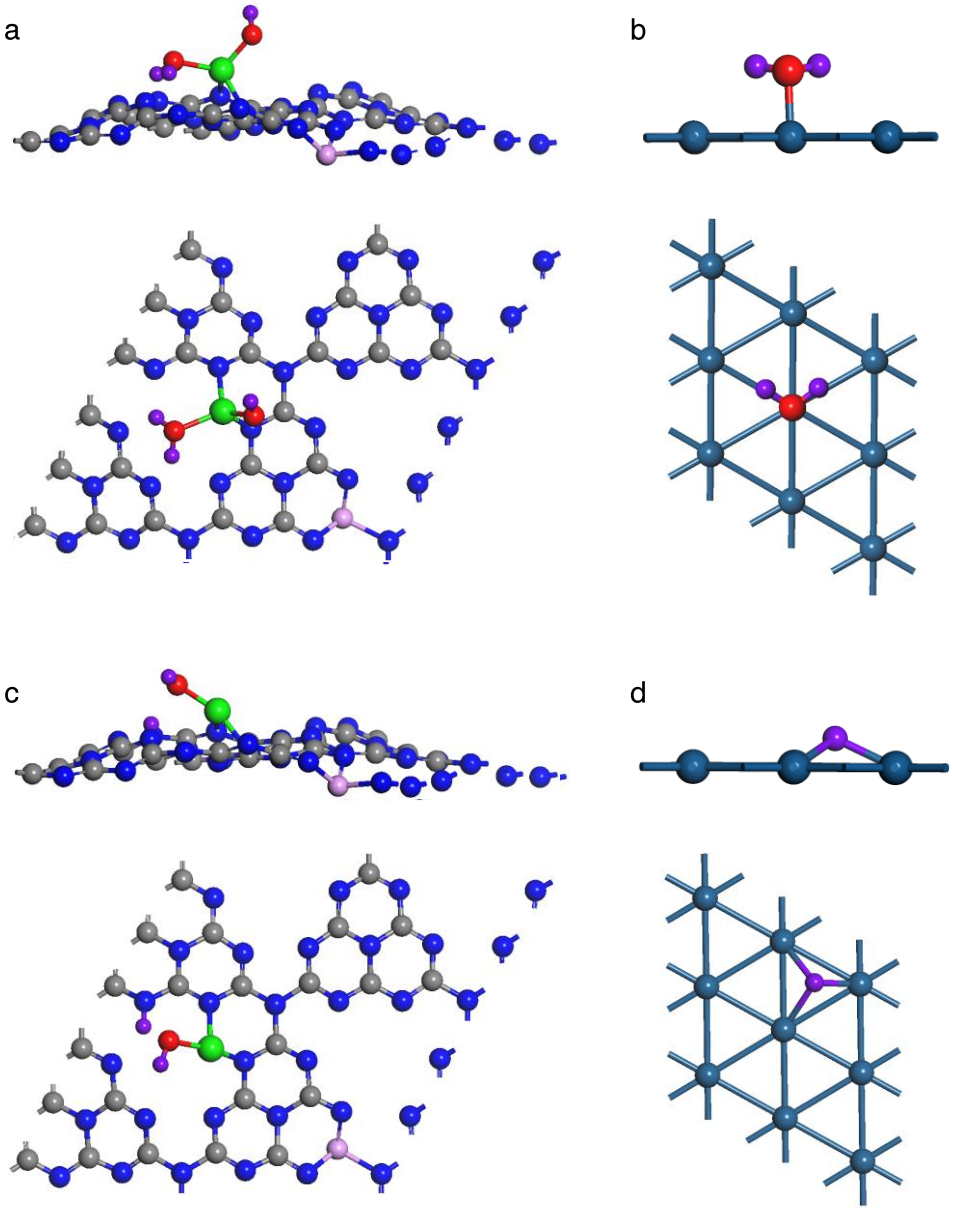


**Supplementary Figure 25.** Top and site views of (a), (b) $H_2O$ adsorption and (c), (d) H adsorption on HO-$Co_1$/PCN and (b) Pt(111). Green, pink, grey, blue, Red, violet and navy blue represent Co, P, C, N, O, H and Pt atoms, respectively.

## Supplementary Tables

**Supplementary Table 1.** Comparisons of the HER activity of the $Co_1$/PCN with other recently reported single-atom catalysts in alkaline solution.

| Ctalysts | Mass loading ($mg/cm^2$) | Overpotential (mV) | Tafel slope ($mV\ dec^{-1}$) | References |
|---|---|---|---|---|
| $Co_1$/PCN | 0.5 | 89 | 59 | Our work |
| $Pt_1$/PCM | 21.4 | 139 | 73.6 | Ref[11] |
| $Mo_1/N_1C_2$ | 0.408 | 132 | 90 | Ref[12] |
| $Pt_1$/NT-NF | 0.14 | 20 | - | Ref[13] |
| $Co_1N_x$/C | 2.0 | 247 | 75 | Ref[14] |
| $Co_1$/NG | 0.285 | 270 | - | Ref[15] |

**Supplementary Table 2**. Structural parameters extracted from quantitative EXAFS curve-fitting using the ARTEMIS module of IFEFFIT (The fixed parameters are underlined).

| Sample | Path | *N* | *R* (Å) | $\sigma^2$ ($10^{-3}$Å$^2$) | $\Delta E_0$ (eV) | *R*-factor |
|---|---|---|---|---|---|---|
| CoO | Co-O | 6 | 2.12 | | | |
| | Co-Co | 12 | 3.00 | | | |
| $Co_3O_4$ | Co-O | 5.3 | 1.91 | | | |
| | Co-$Co_i$ | 4.0 | 2.85 | | | |
| | Co-$Co_{ii}$ | 9.3 | 3.37 | | | |
| *Ex-situ* | Co-$N_i$ | 2.2±0.2 | 2.06±0.02 | 2.0±1.4 | 5.5±1.5 | 0.002 |
| | Co-$N_{ii}$ | 2.1±0.2 | 2.18±0.02 | 2.0±1.4 | 5.5±1.5 | |
| At open circuit | Co-$N_i$ | <u>2.0</u> | 2.01±0.02 | 2.7±1.2 | <u>5.5</u> | 0.001 |
| | Co-$O_i$ | 1.0±0.1 | 2.08±0.02 | 2.7±1.2 | 4.0±1.3 | |
| At -0.04 V | Co-$N_i$ | <u>2.0</u> | 1.99±0.02 | 3.1±1.2 | <u>5.5</u> | 0.001 |
| | Co-$O_i$ | <u>1.0</u> | 2.06±0.03 | 3.1±1.2 | <u>4.0</u> | |
| | Co-$O_{ii}$ | 1.0±0.1 | 2.13±0.03 | 6.2±2.0 | <u>4.0</u> | |
| At -0.1 V | Co-$N_i$ | <u>2.0</u> | 1.99±0.02 | 3.1±1.2 | <u>5.5</u> | 0.007 |
| | Co-$O_i$ | <u>1.0</u> | 2.07±0.03 | 3.1±1.2 | <u>4.0</u> | |
| | Co-$O_{ii}$ | <u>1.0</u> | 2.13±0.03 | 6.2±1.6 | <u>4.0</u> | |

*N*, coordination number; *R*, bond length; $\sigma^2$ Debye-Waller factor; $\Delta E_0$ inner potential shift.

## Supplementary References


1. Ran, J., Ma, T. Y., Gao, G., Du, X.-W. & Qiao, S. Z. Porous P-doped graphitic carbon nitride nanosheets for synergistically enhanced visible-light photocatalytic $H_2$ production. *Energy Environ. Sci.* **8**, 3708-3717 (2015).
2. Gu, H., Gu, Y., Li, Z., Ying, Y. & Qian, Y. Low-temperature route to nanoscale $P_3N_5$ hollow spheres. *J. Mater. Res.* **18**, 2359-2363 (2003).
3. Liu, S., Zhu, H., Yao, W., Chen, K. & Chen, D. One step synthesis of P-doped g-$C_3N_4$ with the enhanced visible light photocatalytic activity. *Appl. Surf. Sci.* **430**, 309-315 (2018).
4. Zhang, Y., Mori, T., Ye, J. & Antonietti, M. Phosphorus-doped carbon nitride solid: enhanced electrical conductivity and photocurrent generation. *J. Am. Chem. Soc.* **132**, 6294-6295 (2010).
5. Guo, S. *et al.* Phosphorus−Doped Carbon Nitride Tubes with a Layered Micro-nanostructure for Enhanced Visible-Light Photocatalytic Hydrogen Evolution. *Angew. Chem. Int. Ed.* **128**, 1862-1866 (2016).
6. Chen, W. *et al.* Rational Design of Single Molybdenum Atoms Anchored on N-Doped Carbon for Effective Hydrogen Evolution Reaction. *Angew. Chem. Int. Ed.* **129**, 16302-16306 (2017).
7. Mahmood, J. *et al.* An efficient and pH-universal ruthenium-based catalyst for the hydrogen evolution reaction. *Nat. Nanotechnol.* **12**, 441-446 (2017).
8. Zhang, J. *et al.* Interface Engineering of $MoS_2/Ni_3S_2$ Heterostructures for Highly Enhanced Electrochemical Overall-Water-Splitting Activity. *Angew. Chem. Int. Ed.* **128**, 6814-6819 (2016).
9. Zheng, Y. *et al.* High electrocatalytic hydrogen evolution activity of an anomalous ruthenium catalyst. *J. Am. Chem. Soc.* **138**, 16174-16181 (2016).
10. Lee, J. H. *et al.* Carbon dioxide mediated, reversible chemical hydrogen storage using a Pd nanocatalyst supported on mesoporous graphitic carbon nitride. *J. Mater. Chem. A* **2**, 9490-9495 (2014).
11. Zhang, H. *et al.* Dynamic traction of lattice-confined platinum atoms into mesoporous carbon matrix for hydrogen evolution reaction. *Sci. Adv.* **4**, eaao6657 (2018).
12. Chen, W. *et al.* Rational Design of Single Molybdenum Atoms Anchored on N−Doped Carbon for Effective Hydrogen Evolution Reaction. *Angew. Chem. Int. Ed.* **129**, 16302-16306 (2017).
13. Zhang, L., Han, L., Liu, H., Liu, X. & Luo, J. Potential-Cycling Synthesis of Single Platinum Atoms for Efficient Hydrogen Evolution in Neutral Media. *Angew. Chem. Int. Ed.* **56**, 13694-13698 (2017).
14. Liang, H. W. *et al.* Molecular metal-$N_x$ centres in porous carbon for electrocatalytic hydrogen evolution. *Nat. Commun.* **6**, 7992 (2015).
15. Fei, H. *et al.* Atomic cobalt on nitrogen-doped graphene for hydrogen generation. *Nat. Commun.* **6**, 8668 (2015).